THE JOURNAL OF PHYSICAL CHEMISTRY B

Article

pubs.acs.org/JPCB

Vibrational Spectroscopy of Structurally Relaxed Self-Trapped Excitons via Excited-State Resonant Impulsive Stimulated Raman Spectroscopy

F. X. Morrissey† and S. L. Dexheimer*

Department of Physics and Astronomy and Materials Science Program, Washington State University, Pullman, Washington 99164-2814, United States

ABSTRACT: We probe the vibrational modes of the equilibrated self-trapped exciton (STE) in the mixed-valence linear chain material $[Pt(en)_2][Pt(en)_2Br_2]\cdot(ClO_4)_4$ using resonantly enhanced impulsive stimulated Raman excitation of the excited electronic state. In these measurements, excitons are created by photoexcitation of the optical intervalence charge transfer band, and after a delay to allow self-trapping and equilibration, the metastable STE is impulsively excited and probed within its red-shifted absorption band. The pump−pump−probe response reveals wavepacket oscillations at a frequency of 125 cm^{-1} that are assigned to a Raman-active mode of the STE having Br−Pt−Br symmetric stretching character. This frequency is shifted from the 171 cm^{-1} symmetric stretch Raman frequency of the ground electronic state, and from the previously observed 110 cm^{-1} wavepacket modulation that accompanies the formation of the STE from the initially excited electronic state, reflecting a new component of the structural relaxation of the exciton.

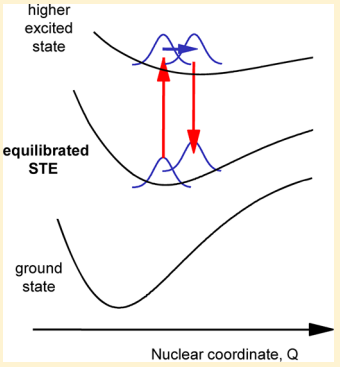

INTRODUCTION

Mixed-valence linear chain materials have proven to be excellent systems for investigating the dynamics of exciton self-trapping. In this process, an initially excited, delocalized free exciton interacts with the lattice to create a localized self-trapped exciton (STE) in which the exciton is stabilized in a localized lattice distortion.[1] In quasi-one-dimensional materials, the linear geometry simplifies the dynamics of the self-trapping process: the electronic excitation is coupled to a limited number of phonon modes of the crystalline lattice, rather than to a thermal bath with a large number of degrees of freedom, allowing a clear observation of the coupled electronic and vibrational dynamics. Theoretical analysis of the dimensionality dependence of the self-trapping process[2] has shown that, in general, two- and three-dimensional systems have a potential barrier between the free and self-trapped states, so that the self-trapping rate is limited by thermal activation or tunneling. In contrast, in an ideal one-dimensional lattice, the transition from the extended free exciton state to the localized STE state is theoretically predicted to be a barrierless process, with the structural rearrangement occurring on the time scale of a single vibrational period of the lattice.

The quasi-one-dimensional geometry of the halide-bridged mixed-valence linear chain (MX) materials is defined by a covalently bonded, extended linear chain of alternating transition metal ions (M) and halide ions (X), as shown schematically in Figure 1. The properties of the ground electronic state are determined by the balance between the electron−electron and electron−phonon interactions. For platinum−halide complexes, the electron−phonon interaction is the dominant effect, and the ground state is a Peierls-distorted commensurate charge density wave with alternating

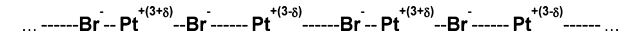

Figure 1. Schematic structure along the platinum−bromide chain axis in the ground electronic state of the PtBr(en) complex, showing two repeat units of the Peierls-distorted charge density wave. Photoexcitation of the optical IVCT transition, which transfers charge between inequivalent Pt sites, triggers the formation of the STE, which corresponds to a localized region in the chain in which the Peierls distortion and the amplitude of the charge density wave are reduced. In PtBr(en), the STE is predicted to extend over ∼5 Pt_2Br_2 repeat units.

valence states on the metal ions and corresponding alternation in the metal−halide bond lengths. For the $[Pt(en)_2][Pt(en)_2Br_2]\cdot(ClO_4)_4$ complex (also abbreviated as PtBr(en); en = ethylenediamine, $C_2H_8N_2$) studied here, the crystalline structure consists of parallel $[Pt(en)_2][Pt(en)_2Br_2]$ chains in which each Pt ion is coordinated by two equatorial ethylenediamine ligands and the chains are separated by ClO_4^- counterions. In PtBr(en), the amplitude of the charge density wave, characterized by the deviation δ from the average Pt valence of +3, is estimated to be $\delta \sim 0.64$ from modeling[3] of XPS measurements,[4] and the extent of the Peierls distortion, as characterized by the ratio of the short $Pt^{+(3+\delta)}$−Br bond length to the long $Pt^{+(3-\delta)}$−Br bond length determined by X-ray diffraction,[5] is $\rho = 0.828$. Covalent bonding involving the Pt $5d_{z^2}$ and Br $4p_z$ orbitals along the chain axis results in a one-

Special Issue: Richard A. Mathies Festschrift

Received: April 6, 2012
Revised: June 28, 2012
Published: July 3, 2012

dimensional electronic band structure, and the optical absorption spectrum is dominated by a strong optical intervalence charge transfer (IVCT) transition that is polarized along the chain axis and that effectively transfers charge between inequivalent metal sites within the chain structure. The final state of this electronic transition, the free exciton, is delocalized along the chain axis, and rapidly evolves to form an STE, which consists of a localized region in which the charge density wave is reduced and the Peierls distortion of the metal−halide bond lengths is accordingly relaxed. The atomic motions that lead to this photoinduced structural change are expected to largely involve those of the Br−Pt−Br Raman-active symmetric stretching mode, which is strongly coupled to the optical IVCT transition owing to the dependence of the Pt−Br bond lengths on the local valence state. For PtBr(en), the localization length, or spatial extent, of the STE is estimated to be approximately five repeat units of the PtBr chain structure, based both on predictions from numerical calculations using an extended Peierls−Hubbard model[6] and from analysis of the coherent acoustic phonon response associated with self-trapping that has been detected at low temperature in this material.[7] Luminescence measurements show a large Stokes shift associated with the formation of the STE, from a peak of 1.9 eV in the optical absorption spectrum of the IVCT transition to a peak of 0.8 eV in the luminescence,[3] indicating that the STE is strongly trapped, and transient absorption measurements yield a lifetime of ∼10 ps for the metastable STE state.[8]

In our initial studies of exciton self-trapping,[8,9] which were carried out on the $[Pt(en)_2][Pt(en)_2Br_2]\cdot(PF_6)_4$ complex, we observed the formation of the STE following excitation of the IVCT transition through the appearance of its characteristic red-shifted optical absorption with a formation time of ∼300 fs, on the order of a single vibrational period of the phonon response. The optical response was found to be strongly modulated by wavepacket oscillations at a frequency of 110 cm^{-1} that damp during the formation of the STE optical absorbance. The 110 cm^{-1} oscillation frequency is absent from the Raman spectrum of the ground state of the complex and is strongly shifted from the 175 cm^{-1} frequency of the Raman-active Br−Pt−Br symmetric stretching mode of the ground electronic state. Measurements of the transient absorption response at wavelengths throughout the STE absorption spectrum provided a picture of the excited state dynamics in which the 110 cm^{-1} oscillation corresponds to a lattice motion that carries the photoexcited system from the initial ground state structure toward the structure that stabilizes the STE.[9] Remarkably, these wavepacket oscillations give a nearly 100% modulation of the formation of the STE absorption spectrum, indicating that the motion associated with the 110 cm^{-1} oscillation is the dominant contribution to the self-trapping process. Measurements on the $[Pt(en)_2][Pt(en)_2Br_2]\cdot(ClO_4)_4$ complex, which differs only in the counterion that separates parallel $[Pt(en)_2][Pt(en)_2Br_2]$ chains in the crystal structure and is the material investigated in the present study, have shown essentially identical dynamics, and moreover, the same phenomenology for exciton self-trapping dynamics has been observed in a series of platinum−halide linear chain complexes in which the bridging halide ion X = Cl, Br, or I controls the strength of the electron−phonon coupling and the degree of electronic delocalization: in all cases, a red-shifted induced absorbance associated with the STE forms on a time scale of a single vibrational period of a short-lived excited-state wavepacket oscillation, with the time scale of the STE formation and the extent of the frequency shift of the excited-state wavepacket from the ground state Raman frequency varying systematically with the electronic and lattice properties determined by the identity of the halide bridging group.[9−11]

A number of time-resolved luminescence and transient absorption measurements on MX materials have now shown excited-state wavepacket motion associated with exciton self-trapping;[7−16] however, a key component of the evolution of the coupled electron−lattice system is missing from these measurements. In all of these previous impulsive excitation studies, the excited-state wavepacket motion reflects the initial vibrational dynamics of the photoexcited system, and since the oscillations dephase as the STE forms and relaxes, information on the vibrational properties of the exciton is lost as it evolves to its final equilibrated structure. An important issue that remains for a complete understanding of the physics of the localization process is the nature and evolution of the internuclear potential as the lattice distorts to stabilize the electronic excitation and form the final structurally relaxed self-trapped state. Toward this end, we present here a pump−pump−probe method that provides a time-domain Raman probe of the vibrational properties of the STE in its final equilibrated structure. In these experiments, an initial pump pulse excites the IVCT transition to generate a population of excitons. After a time delay to allow equilibration, a second pump pulse spectrally shifted to lie within the red-shifted STE absorption band impulsively excites the STE. The resulting wavepacket motion is detected as a function of time delay between the second pump and the probe pulse, and the response originating from the excited state is detected by lock-in amplification with simultaneous modulation of both pump beams. This response includes an oscillatory component at the frequency of the Raman-active mode of the STE, generated by the resonant impulsive stimulated Raman mechanism *acting on the excited state.* A schematic wavepacket diagram showing the Raman process originating in the excited state is presented in Figure 2.

Generation of coherent vibrational motion via the resonant impulsive stimulated Raman process originating in the *ground* electronic state is nearly ubiquitous in pump−probe measurements in the vibrationally impulsive limit. Modeling of this process using a $\chi^{(3)}$ formalism with displaced harmonic potential response functions has predicted oscillatory modulation of the transient absorption with significant modulation amplitude for a wide range of excitation pulse durations, with maximal wavepacket oscillation amplitude for an excitation pulse duration ∼30% of the vibrational period.[17] The resonant impulsive stimulated Raman wavepacket response shows a characteristic dependence on detection wavelength in wavelength-resolved measurements: the oscillation amplitude peaks around probe wavelengths corresponding to energies that are one vibrational quantum to the red and blue of the center of the probe pulse spectrum, and the oscillations show an antiphased response at the red and blue sides of the probe pulse spectrum under typical conditions. Wavepacket oscillations resulting from impulsive stimulated Raman excitation can be detected over a wide spectral range, including spectral regions well outside of the ground state absorption spectrum.[17−19]

Multiple pulse impulsive excitation techniques have proven useful in probing changes in low-frequency excited state vibrational frequencies in a variety of contexts. For example, Takeuchi et al.[20] probed the frequency of a spectator mode during a photoisomerization reaction by impulsive excitation of

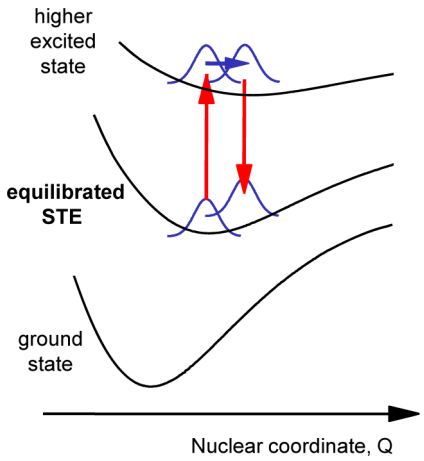

Figure 2. Resonant impulsive stimulated Raman excitation of vibrational wavepacket motion in the excited electronic state. The first interaction with the field of a resonant optical pump pulse that is short compared to a vibrational period brings a wavepacket up to a higher-lying electronic state, where it propagates on the upper surface within the duration of the pulse. A second interaction with the pump field brings the wavepacket back down to the STE surface, creating a nonstationary vibrational state that oscillates at the characteristic frequency of the equilibrated STE. The nuclear coordinate for the various schematic potential energy surfaces involves Br–Pt–Br stretching motion but is not necessarily identical for all of the surfaces.

the photoexcited state, and more recently, Trigo et al.[21] reported softening of a Raman-active phonon mode in a photoexcited perovskite material using a pump–pump–probe sequence. Here, we use a pump–pump–probe sequence to carry out an excited-state resonant impulsive stimulated Raman measurement of the structurally active vibrational motion of an STE, and introduce a double-modulation detection scheme to isolate the signal originating from the excited state. This time-domain excited-state Raman measurement allows us to detect vibrational modes in a time and frequency range that can be difficult to access with established time-resolved Raman methods.[22] In these measurements, the initial pump pulse generates the population of excitons, using excitation at the low energy edge of the IVCT band at 800 nm to minimize excess vibrational energy in the initially excited state. The duration of the first pump pulse is relatively long, 120 fs, so as to produce minimal wavepacket modulation in the initially excited population. The second pump pulse, used for impulsive stimulated Raman excitation of the excited state population, has a spectrum centered at 1.31 μm, which is chosen to lie within the red-shifted absorption spectrum of the STE for resonant enhancement of the Raman response, while falling well outside of the optical IVCT transition so as to avoid excitation from the ground electronic state. The 45 fs duration of the second pump pulse yields significant impulsive stimulated Raman excitation for the expected vibrational frequency range. The probe pulse is degenerate with the second pump pulse, and is wavelength resolved following interaction with the sample to enhance detection of the Raman oscillations. Using this approach, we find a shift in the vibrational frequency between the initially excited and equilibrated self-trapped states, revealing a new component of the structural relaxation of the coupled electron–lattice system.

EXPERIMENTAL METHODS

Excited-state resonant impulsive stimulated Raman measurements were carried out using optical pulses derived from the output of a Spectra-Physics Hurricane amplified Ti:sapphire system producing pulses 120 fs in duration centered at 800 nm at a repetition rate of 1 kHz. A portion of the 120 fs, 800 nm amplifier output was used as the first pump pulse to generate the exciton population, and the remainder was used to pump an IR optical parametric amplifier. The OPA signal output at 1.31 μm was compressed with a pair of fused silica prisms to a duration of 45 fs and was passed through a beamsplitter to generate the second pump pulse and the probe pulse. The wavepacket motion resulting from impulsive excitation of the equilibrated STE by the second pump pulse is detected as a function of time delay between the second pump and the probe pulse. Detection of the response originating from the excited state is achieved by simultaneously chopping both pump beams at different chopping rates using a dual-frequency chopper wheel and observing the probe intensity at the sum of the individual modulation frequencies using a lock-in amplifier. This detection scheme allows a clear measurement of the vibrational response of the equilibrated STE because the measurement will be sensitive to only the differential changes requiring the presence of both pump pulses (i.e., $\Delta(\Delta T/T)$) and is insensitive to the individual pump responses. The sensitivity of the measurements was enhanced by splitting off a small portion of the 1.31 μm pulse for use as a separately detected reference to correct for intensity fluctuations of the probe pulses. Both the probe and reference beams were passed through a grating monochromator and were detected using a pair of matched InGaAs photodiodes. Transient absorption measurements were also carried out using a single-pump–probe pulse sequence with a 120 fs, 800 nm pump and 45 fs, 1.31 μm probe, and with identical 45 fs, 1.31 μm pulses as the pump and probe, to allow comparison with the double-modulated pump–pump–probe response. To allow comparison with the wavepacket dynamics associated with the initial self-trapping dynamics, additional transient absorption measurements using 800 nm excitation were carried out in the impulsive excitation limit with a separate 35 fs, 1 kHz amplified Ti:sapphire system. These measurements were carried out using a compressed continuum as the probe, as described previously.[8,9]

Oriented single-crystal samples of $[Pt(en)_2][Pt(en)_2Br_2]\cdot(ClO_4)_4$ were mounted on 1 mm thick sapphire plates, and were maintained at room temperature. Synthesis was carried out using methods that produce crystals that are largely free of defects and that are resistant to photoinduced damage.[23,24] Transient absorption measurements were carried out with the pump and probe fields polarized along the chain axis. As expected from the nature of the optical transitions, no transient absorption signals were detected for polarization of the pump fields perpendicular to the chain axis, or for polarization of the probe field perpendicular to that of the pumps.

The components of the measured response were analyzed using a number of independent methods, including Fourier analysis, linear prediction/singular value decomposition (LPSVD), and nonlinear fitting in which the differential transmittance signals are fit to a sum of exponentially damped cosine wave and decaying exponentials, which is the same functional form that is inherent to the LPSVD signal processing

technique. In general, successful multiparameter nonlinear fitting requires a careful choice of initial parameter values. For the analysis presented here, the number of oscillatory components and their starting parameters were determined by the LPSVD and Fourier analysis, and the three methods for determination of the frequency components yielded consistent results.

RESULTS AND DISCUSSION

To distinguish between the wavepacket responses originating from self-trapping of the initially generated exciton, from the structurally relaxed STE, and from impulsive stimulated Raman excitation of ground electronic state, we present measurements carried out under a series of conditions. First, we present single-pump−probe measurements of the initial self-trapping dynamics of the exciton resulting from excitation of the optical IVCT transition in the vibrationally impulsive limit using 35 fs, 800 nm pulses. We then present single-pump−probe measurements carried out with the 120 fs, 800 nm pump pulse and 45 fs, 1.31 μm probe pulse, demonstrating that the same components are present, though with substantially reduced wavepacket amplitude, and characterizing the response at the 1.31 μm wavelength to be used for the second pump pulse in the pump−pump−probe measurements. Next, pump−pump−probe measurements at detection wavelengths on the blue and red sides of the probe pulse spectrum are presented, revealing the Raman frequency of the relaxed STE. Finally, single-pump−probe measurements using 45 fs, 1.31 μm pulses characterize the stimulated impulsive Raman response of the ground electronic state at this excitation wavelength, and also serve to demonstrate that the excited-state Raman frequency component is absent under single-pump 1.31 μm excitation.

I. Initial Self-Trapping Dynamics. *(a). Impulsive Excitation with 35 fs 800 nm Pump.* Figure 3a shows the time-resolved response following excitation of the optical IVCT with a 35 fs pump pulse centered at 800 nm, probed at a detection wavelength of 940 nm, which lies within the red-shifted absorption band of the STE. Signals are presented as the pump-induced change in transmittance, $\Delta T/T$. The components from the fit to a sum of an exponential formation component and exponentially damped cosine oscillations are presented in Figure 3b. The exponential formation component reflects the formation of the STE induced absorbance on a time scale of ~300 fs. The induced absorbance is modulated by a rapidly damped excited state vibrational wavepacket oscillation at a frequency of 110 cm^{-1} that gives a nearly 100% modulation of the signal. The pump−probe response is also modulated by ground state wavepacket oscillations generated by the resonant impulsive stimulated Raman mechanism that appear at the ground state Raman frequency[24,25] of 171 cm^{-1} and its second harmonic at 342 cm^{-1}. The observed response is consistent with transient absorption measurements of the self-trapping dynamics reported[8,9] for the closely related material $[Pt(en)_2]$-$[Pt(en)_2Br_2]\cdot(PF_6)_4$, and by comparison with the previous studies, the 110 cm^{-1} wavepacket oscillation is assigned to the lattice motion that carries the initially photoexcited system from the ground state Franck−Condon structure toward the structure that stabilizes the self-trapped state.

(b). Excitation with 120 fs 800 nm Pump. The response of PtBr(en) to a single pump pulse of 120 fs duration centered at 800 nm and probed within the red-shifted STE absorption spectrum with a 45 fs pulse centered at 1.31 μm is presented in Figure 4a, and the oscillatory components from the fit to a sum

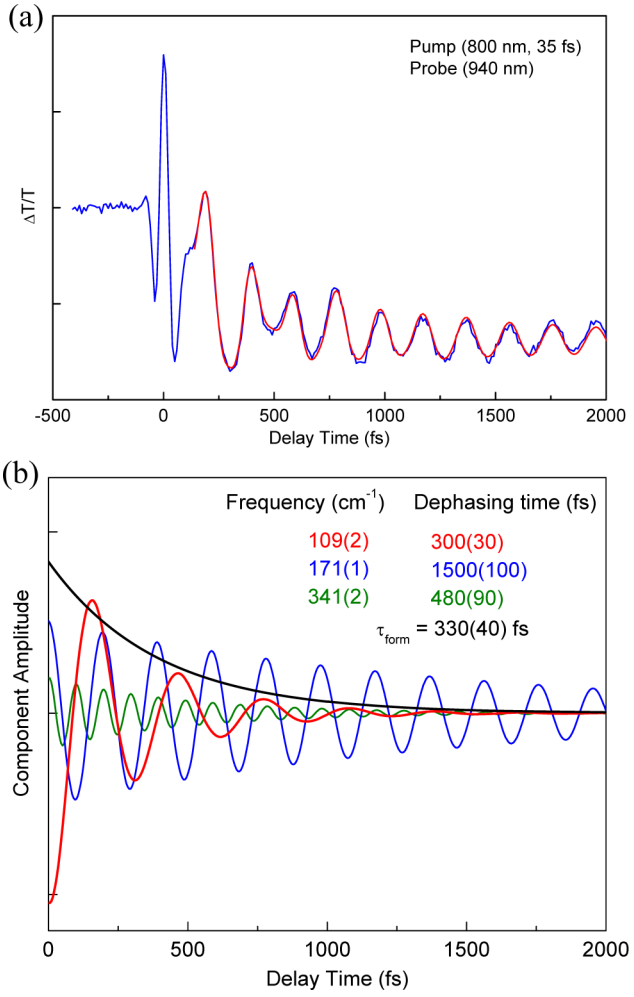

Figure 3. (a) The initial self-trapping dynamics of PtBr(en) as detected in a time-resolved differential transmittance measurement following impulsive excitation of the optical IVCT transition with a single 800 nm, 35 fs pump pulse and probed with a compressed continuum at a detection wavelength of 940 nm, within the red-shifted absorption spectrum of the STE. The red line represents a fit to decaying exponentials and a sum of exponentially damped cosine waves. (b) Components extracted from the fit, including the exponential formation of the STE absorbance, the excited state wavepacket oscillation at 110 cm^{-1}, and oscillations at the ground state Raman frequency of 171 cm^{-1} and its second harmonic at 342 cm^{-1}. For clarity, the long-term decay component is omitted. Numbers in parentheses represent estimated errors in the reported fit parameter values.

of exponentially damped cosine oscillations and an exponential decay are presented in Figure 4b. As expected, given the longer pulse durations used in this measurement, the wavepacket modulation is strongly reduced in amplitude, especially for the higher-frequency ground state Raman mode. The initial formation of the STE absorption is not well resolved in this measurement because of its overlap with the pump−probe pulse overlap features and the initial wavepacket oscillations.

II. Vibrational Response of the Equilibrated STE. Figures 5 and 6 present pump−pump−probe measurements in which the first pump pulse (800 nm, 120 fs, $T = -1$ ps) excites the IVCT transition to generate a population of excitons, and after a delay of 1 ps to allow relaxation of the population to the equilibrated self-trapped structure and decay of the small wavepacket response generated by the initial pump

dx.doi.org/10.1021/jp303288s | J. Phys. Chem. B 2012, 116, 10582−10589

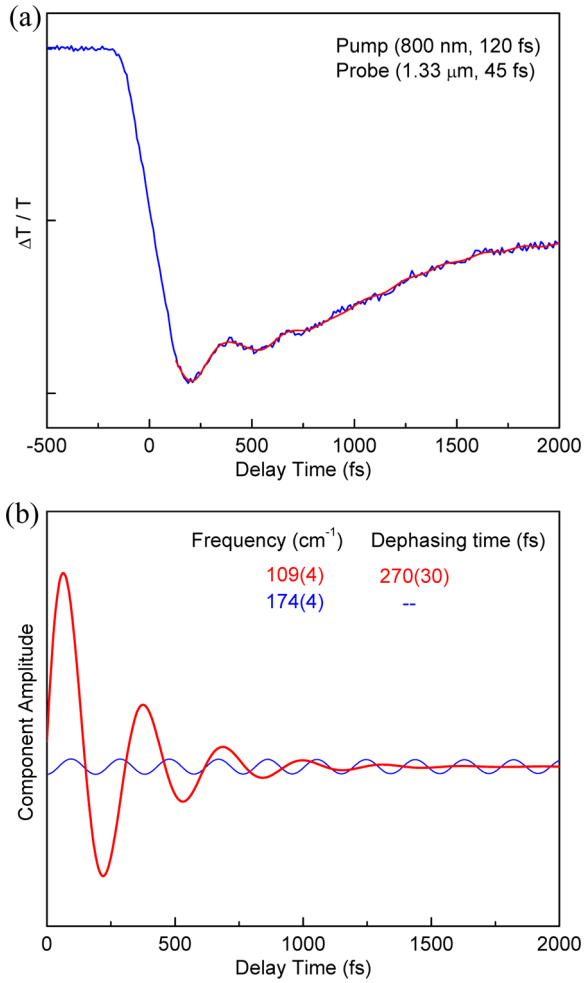

Figure 4. (a) Time-resolved differential transmittance of PtBr(en) following excitation of the optical IVCT transition with a single 800 nm, 120 fs pump pulse and probed with a 1.31 μm, 45 fs probe pulse at a detection wavelength of 1.33 μm, together with a fit to a sum of exponentially damped cosine waves and a decaying exponential. The longer pulse durations result in significantly diminished wavepacket modulation. (b) Oscillatory components of the fit, including the rapidly damped excited state component and a very low amplitude ground state Raman component, for which the dephasing time is not well determined.

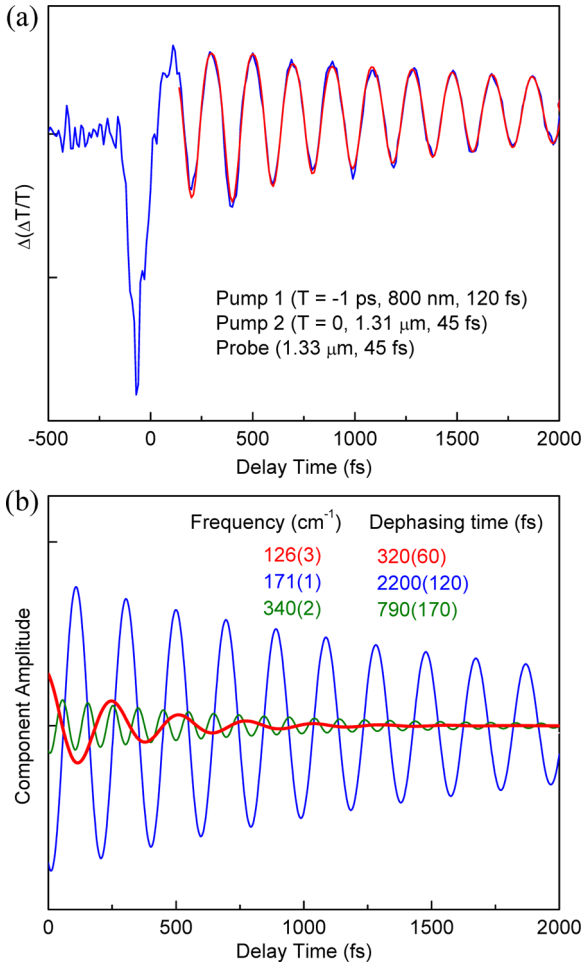

Figure 5. (a) Resonant impulsive stimulated Raman response of the equilibrated STE measured using a pump−pump−probe sequence: pump 1 ($T = -1$ ps, 800 nm, 120 fs), pump 2 ($T = 0$, 1.31 μm, 45 fs), probe (variable delay, 1.31 μm, 45 fs), at a detection wavelength of 1.33 μm, on the red side of the probe pulse spectrum. The red line is a fit to a sum of exponentially damped cosine waves and a decaying exponential background. Signals near zero delay include features from nonlinear interaction of the overlapped pump and probe pulses, and include additional noise due to interference of the probe field with a small amount of scattered pump light at the detector. (b) Oscillatory components of the fit, including a new frequency at 125 cm^{-1} assigned to the equilibrated STE and components at the ground state Raman frequency and its second harmonic.

pulse, the second pump pulse (1.31 μm, 45 fs, $T = 0$) impulsively excites the relaxed STE population. The resulting wavepacket motion is detected as a function of time delay between the second pump pulse and the probe pulse. The response at a detection wavelength of 1.33 μm, on the red side of the probe pulse spectrum, is presented in Figure 5a, with the components of the fit to a sum of exponentially decaying cosine oscillations and a decaying exponential background presented in Figure 5b. The corresponding results at a detection wavelength of 1.29 μm, on the blue side of the probe pulse spectrum, are presented in Figure 6. The overall sign of the doubled modulated $\Delta(\Delta T/T)$ signal is not well determined in these measurements; however, the relative sign of the response at the two different detection wavelengths is well determined. The double-modulated response reveals a new frequency at 125 cm^{-1} in addition to the Raman-active ground state symmetric stretch mode at 170 cm^{-1} and its second harmonic at 340 cm^{-1}.

We assign the new frequency component at 125 cm^{-1} to a Raman-active vibrational mode of the *equilibrated* STE. Detection at the red and blue sides of the probe spectrum yields an antiphased response, as expected for the impulsive stimulated Raman mechanism, and consistent with the assignment of the 125 cm^{-1} component to a vibrational wavepacket oscillation generated by this mechanism acting on the equilibrated STE, as shown schematically in Figure 2. The observed dependence of the phase of the 125 cm^{-1} oscillation on detection wavelength argues against an assignment to wavepacket motion associated with population of a higher-lying electronic state by absorption of the second pump pulse, because wavepacket motion on such a surface would be unlikely to yield this large change in oscillation phase over the relatively small energy difference between the two detection wavelengths. By the same argument, the dependence of the oscillation phase on detection wavelength argues against an assignment to wavepacket motion on the ground electronic state resulting

dx.doi.org/10.1021/jp303288s | J. Phys. Chem. B 2012, 116, 10582−10589

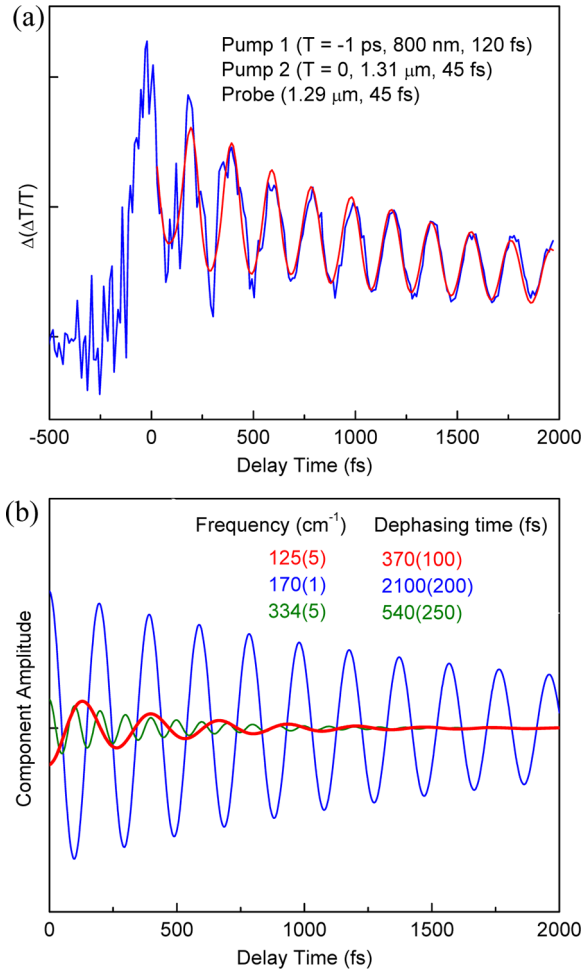

Figure 6. (a) Resonant impulsive stimulated Raman response of the equilibrated STE generated as in Figure 5 and measured at a detection wavelength of 1.29 μm, on the blue side of the probe pulse spectrum, together with a fit to a sum of exponentially damped cosine waves and a decaying exponential background. (b) Oscillatory components of the fit.

from population of a highly anharmonic region of the ground state potential energy surface by the second pump pulse via a stimulated emission pumping mechanism. Further, we note that additional measurements carried out using the same pump−pump−probe sequence, but with the second pump and probe pulses centered at 950 nm rather than 1.31 μm, yield the same oscillation frequency, within error (data not shown). This result also argues against a ground state wavepacket generated by stimulated emission pumping as the origin of the 125 cm^{-1} oscillation, because the 950 nm pump wavelength would access a lower-lying, and therefore less anharmonic, region of the ground state potential energy surface than the 1.31 μm pump wavelength, so that a change in the observed oscillation frequency would be expected under such a mechanism.

The double-modulated response also includes oscillatory components at the frequencies of the ground state symmetric stretch mode fundamental at 170 cm^{-1} and its second harmonic at 340 cm^{-1}. These ground state Raman components likely appear in the double-modulated response as a result of modulation of the ground state population by the first pump pulse, which then changes the amplitude of the detected impulsive stimulated Raman ground state response generated by the second pump pulse.

III. Impulsive Stimulated Raman Response from Off-Resonant Excitation of the Ground Electronic State at 1.31 μm. The time-resolved differential transmittance using a single 45 fs pump pulse centered at 1.31 μm and probed with an identical pulse at a detection wavelength of 1.33 μm is presented in Figure 7a, and the oscillatory components from

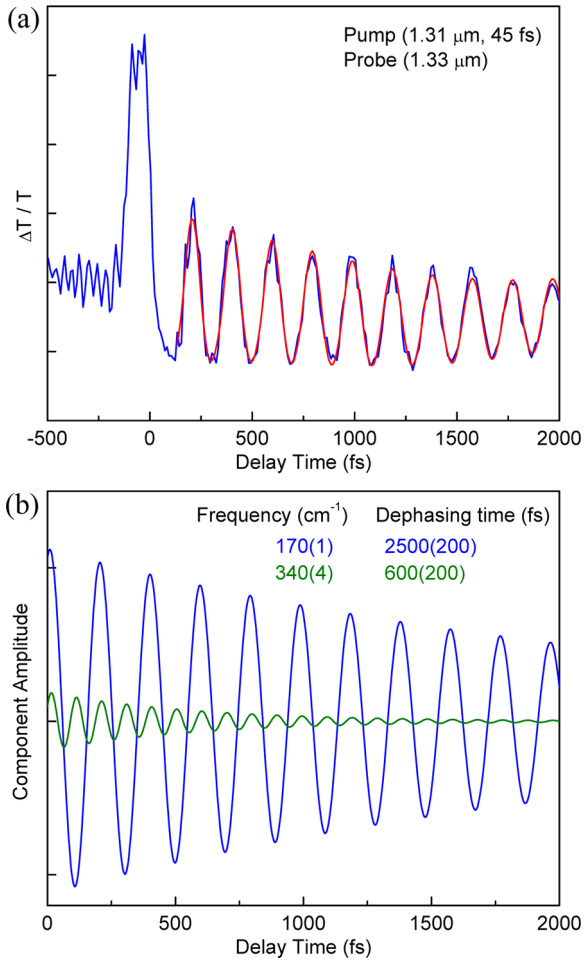

Figure 7. (a) Time-resolved differential transmittance of PtBr(en) following excitation with a single 1.31 μm, 45 fs pump pulse and probed with 1.31 μm, 45 fs at a detection wavelength of 1.33 μm, together with a fit to a sum of exponentially damped cosine waves and a decaying exponential background. (b) Oscillatory components of the fit. The off-resonant excitation results in wavepacket modulation only at the ground state Raman frequency and its second harmonic; the 125 cm^{-1} component detected in the double-modulated pump−pump−probe response is absent.

the fit to a sum of exponentially decaying cosine oscillations and a decaying exponential background are presented in Figure 7b. As expected for this off-resonant excitation wavelength, only the ground state Raman response is observed, with the fundamental of the symmetric stretch mode appearing at 170 cm^{-1} and its second harmonic at 340 cm^{-1}. The small monotonic background signal may result from two-photon excitation of a higher-lying electronic state. No evidence of the 125 cm^{-1} component is found in the single-pump response, verifying that this frequency component originates from the excited state population in the double-modulated response.

IV. Implications for the Vibrational Dynamics. The series of measurements presented above establish the Raman

dx.doi.org/10.1021/jp303288s | J. Phys. Chem. B 2012, 116, 10582−10589

frequency of the equilibrated STE as 125 cm^{-1}. This frequency is observed only in the double-modulated two-pump signal, and results from resonant impulsive stimulated Raman excitation of the relaxed excited state. The vibrational motion corresponding to this mode is expected to have Br−Pt−Br symmetric stretching character. The properties of the metastable electronic excitations in PtBr(en) have been modeled by numerical calculations based on an extended Peierls−Hubbard Hamiltonian with parameters estimated from structural and spectroscopic properties of the complex, and the equilibrated STE is predicted to extend over 5 Pt_2Br_2 units of the chain structure.[6] Experimental evidence for this spatial extent of the STE comes from impulsive excitation measurements at low temperature that reveal a signature of acoustic mode coupling to the self-trapping process, with a dominant contribution from phonons of wavelength on the order of the spatial extent of the STE.[7] The envelope of the STE electronic wave function, and, correspondingly, of the region over which the chain structure is distorted, is predicted to vary smoothly over the ∼5 Pt_2Br_2 units to define a localized region in which the charge density wave and Peierls distortion are reduced, with a deviation from the ground state that is largest in the center of the envelope and becomes smaller in the tails of the wave function envelope. The vibrational modes of this structure are expected to be more complex than those of the ground state, though a mode with Raman activity that maintains a Br−Pt−Br symmetric stretching character similar to that of the strong Raman-active mode of the ground electronic state is expected to be present. The lower frequency of the 125 cm^{-1} mode of the STE relative to the 171 cm^{-1} frequency of the ground electronic state may be expected to result from the change in charge distribution in the STE, where the weaker charge density wave results in reduced force constants. The rapid dephasing observed for the 125 cm^{-1} oscillation could result from a distribution of closely spaced Raman-active modes, or from a limited vibrational lifetime due to coupling to other modes of the STE or the lattice in which it is embedded. Future measurements at low temperature may elucidate the relative contributions of these effects if thermal contributions to the dephasing are significant.

The observation of a shift in vibrational frequency associated with equilibration of the STE is an intriguing result that provides further insight into the self-trapping process. In the measurements presented in Figure 3, the initial formation of the STE in PtBr(en) following single-pump impulsive excitation of the IVCT is accompanied by a strongly damped wavepacket oscillation of frequency 110 cm^{-1} that decays as the characteristic red-shifted absorbance of the STE appears on a time scale of ∼300 fs. In the double-modulated pump−pump−probe measurements presented in Figures 5 and 6, we find that the vibrational frequency of the equilibrated STE has shifted to higher frequency, 125 cm^{-1}, indicating that further structural relaxation takes place during the evolution of the system from the initial photoexcitation to the equilibrated structure of the self-trapped state. The nature of the dynamics that lead to the change in frequency of the equilibrated state and to the dephasing of the initial vibrational coherence will be issues of interest to address in future studies.

CONCLUSION

We have presented excited-state resonant impulsive stimulated Raman measurements of the structurally active vibrational mode of an equilibrated STE. The impulsive stimulated Raman process allows the detection of excited-state frequencies in a range not readily accessible via other time-resolved Raman techniques, and our approach allows signals originating from the excited state to be isolated using double-modulation detection. The measurements provide a probe of structural evolution associated with exciton self-trapping that extends beyond the initial vibrational coherence of the initially photoexcited state. In particular, we find that the vibrational frequency of the structurally active mode of the STE in PtBr(en) shifts upon equilibration to 125 cm^{-1} from the 110 cm^{-1} frequency of the initially excited electronic state, revealing a new component of the structural relaxation inherent to the localization process. These results motivate further experiments to probe the structural evolution throughout the self-trapping process in the excited state.

AUTHOR INFORMATION

Corresponding Author

*E-mail: dexheimer@wsu.edu.

Present Address

[†]MIT Lincoln Laboratory, Lexington, MA.

Notes

The authors declare no competing financial interest.

ACKNOWLEDGMENTS

This work was supported by the National Science Foundation under grants DMR-0706407 and DMR-0305403. We thank W. E. Buschmann for preparing the single-crystal samples of the PtBr(en) complex.

REFERENCES

(1) Rashba, E. I. Self-trapping of excitons. In *Excitons*; Rashba, E. I., Sturge, M. D., Eds.; North-Holland: New York, 1982; p 543.
(2) Emin, D.; Holstein, T. *Phys. Rev. Lett.* **1976**, *36*, 323.
(3) Wada, Y.; Mitani, T.; Yamashita, M.; Koda, T. *J. Phys. Soc. Jpn.* **1985**, *54*, 3143.
(4) Yamashita, M.; Matsumoto, N.; Kida, H. *Inorg. Chim. Acta* **1978**, *31*, L381.
(5) Huckett, S. C.; Scott, B.; Love, S. P.; Donohoe, R. J.; Burns, C. J.; Garcia, E.; Frankcom, T.; Swanson, B. I. *Inorg. Chem.* **1993**, *32*, 2137.
(6) Gammel, J. T.; Saxena, A.; Batistic, I.; Bishop, A. R.; Phillpot, S. R. *Phys. Rev. B* **1992**, *45*, 6408.
(7) Morrissey, F. X.; Dexheimer, S. L. *Phys. Rev. B* **2010**, *81*, 094302.
(8) Dexheimer, S. L.; Van Pelt, A. D.; Brozik, J. A.; Swanson, B. I. *J. Phys. Chem. A* **2000**, *104*, 4308.
(9) Dexheimer, S. L.; Van Pelt, A. D.; Brozik, J. A.; Swanson, B. I. *Phys. Rev. Lett.* **2000**, *84*, 4425.
(10) Morrissey, F. X. Ph.D. thesis, Washington State University, Morrissey, F. X et al., manuscript in preparation
(11) Van Pelt, A. D.; Dexheimer, S. L. In *Ultrafast Phenomena XII, Springer Series in Chemical Physics*, Vol. *66*; Elsaesser, T., Mukamel, S., Murnane, M., Scherer, N. F., Eds.; Springer-Verlag: Berlin, 2001; p 393.
(12) Tomimoto, S.; Saito, S.; Suemoto, T.; Sakata, K.; Takeda, J.; Kurita, S. *Phys. Rev. B* **1999**, *60*, 7961.
(13) Tomimoto, S.; Saito, S.; Suemoto, T.; Takeda, J.; Kurita, S. *Phys. Rev. B* **2002**, 66.
(14) Yasukawa, K.; Takahashi, Y.; Kurita, S.; Suemoto, T. *Solid State Commun.* **2006**, *140*, 197.
(15) Sugita, A.; Saito, T.; Kano, H.; Yamashita, M.; Kobayashi, T. *Phys. Rev. Lett.* **2001**, *86*, 2158.
(16) Wada, Y.; Matsushita, N.; Haneda, H. *J. Lumin.* **2004**, *108*, 285.
(17) Pollard, W. T.; Dexheimer, S. L.; Wang, Q.; Peteanu, L. A.; Shank, C. V.; Mathies, R. A. *J. Phys. Chem.* **1992**, *96*, 6147.
(18) Dhar, L.; Rogers, J. A.; Nelson, K. A. *Chem. Rev.* **1994**, *94*, 157.

(19) Kumar, A.; Rosca, F.; Widom, A.; Champion, P. *J. Chem. Phys.* **2001**, *114*, 701.
(20) Takeuchi, S.; Ruhman, S.; Tsuneda, T.; Chiba, M.; Taketsugu, T.; Tahara, T. *Science* **2008**, *322*, 1073.
(21) Trigo, M.; Chen, J.; Jiang, M. P.; Mao, W. L.; Riggs, S. C.; Shapiro, M. C.; Fisher, I. R.; Reis, D. A. *Phys. Rev. B* **2012**, *85*, 081102.
(22) McCamant, D. W.; Kukura, P.; Yoon, S.; Mathies, R. A. *Rev. Sci. Instrum.* **2004**, *75*, 4971 and references cited therein.
(23) Brozik, J. A.; Scott, B. L.; Swanson, B. I. *Inorg. Chem. Acta* **1999**, *294*, 275.
(24) Buschmann, W. E.; McGrane, S. D.; Shreve, A. P. *J. Phys. Chem. A* **2003**, *107*, 8198.
(25) Clark, R. J. H. Raman and resonance Raman spectroscopy of linear chain complexes. In *Advances in Infrared and Raman Spectroscopy*; Clark, R. J. H., Hester, R. E., Eds.; Wiley: New York, 1984; Vol. *11*, p 95.